Journal of ELECTRONIC MATERIALS, Vol. 48, No. 7, 2019
https://doi.org/10.1007/s11664-019-07185-8
© 2019 The Minerals, Metals & Materials Society

# Lower Band Gap Sb/$ZnWO_4$/r-GO Nanocomposite Based Supercapacitor Electrodes

K. BRIJESH[1,2] and H.S. NAGARAJA[1,3]

1.—Department of Physics, National Institute of Technology Karnataka, P.O. Srinivasnagar, Surathkal, Mangaluru 575025, India. 2.—e-mail: brijeshphy89@gmail.com. 3.—e-mail: nagaraja@nitk.edu.in

Sb/$ZnWO_4$/r-GO nanocomposite has been prepared by a single step solvothermal method. The crystal structure of the prepared nanocomposite has been characterized using a powder x-ray diffractometer (XRD). The optical properties of the prepared nanocomposite were studied using UV–visible spectroscopy and photoluminescence. The energy band gap of 3.52 eV is obtained for the ZWS-5 nanocomposite using Tauc plots. For both Sb/$ZnWO_4$ and Sb/$ZnWO_4$/r-GO nanocomposite XRD shows the monoclinic Wolframite structure. The supercapacitor performance of the prepared samples was carried out using electrochemical techniques such as cyclic voltammetry, galvanostatic charge–discharge and electrochemical impedance spectroscopy. The nanocomposite ZWS-5 exhibits a specific capacitance of 102 F/g, which is higher than pristine ZWS specific capacitance of 64 F/g. Both ZWS and ZWS-5 electrodes show good capacitance retention proficiency even after 1000 cycles.

**Key words:** Nanocomposites, supercapacitor, Sb/$ZnWO_4$/r-GO

## INTRODUCTION

The energy problem is one of the current issues for mankind due to technology development, limited availability of fossil fuels and a rapidly growing population. Energy production and storage is a million dollar market. In recent years, the main challenge is to provide a sufficient and reliable storage of energy. Supercapacitors and lithium ion batteries are widely used for energy storage.[1,2] Due to faster charge and discharge process, high power density and good cycle stability supercapacitors are an alternative to conventional batteries[3,4]. The performance of the supercapacitors mainly depends upon the electrode materials. Carbon-based materials,[5–9] conducting polymers,[10–16]nitrides,[17–22] carbides,[23–27] and transition metal oxides [28–33] are widely used electrodes for supercapacitors. Carbon based nanomaterial electrodes are good candidates for the supercapacitors due to their good electrical conductivity, wide range of operating temperature, chemical stability and high surface area.[34–37] But low specific capacity of the carbon based electrodes limit their practical usage.[28] The main challenge for supercapacitors is to build a new electrode material with a good cyclic stability and high power density for practical application.

The relation between the band gap and supercapacitance of the materials is one of the interesting topics to further investigate. There are many works reported on the basis of band gap and supercapacitance. Shouzhi Wang et al.,[38] prepared a Porous Borocarbonitrides Nanosheets with tuning the band gap for a supercapacitor application. As they concluded that lower band gap BCN provides the good specific surface area, massive active sites and excellent conductivity which provides high specific capacitance and good stability. Also, Sanjit Saha et al.,[39,40] prepared a band gap altered NiO/$Fe_3O_4$ nanostructure with boron doping for supercapacitor application and also prepared h-BN/rGO composites to study the band structure and electrochemical properties. These works show that, a lower band gap material shows a higher specific capacitance

(Received January 3, 2019; accepted April 2, 2019; published online April 10, 2019)

when compared to a higher band gap material. The present work discusses the enhancement of specific capacitance of Sb/$ZnWO_4$ by the incorporation of r-GO, which reduces the band gap. Here we report lower band gap Sb/$ZnWO_4$/r-GO nanocomposites with high capacitance. As far as we know, there is no report on Sb/$ZnWO_4$/r-GO nanocomposites for a supercapacitor application.

## EXPERIMENTAL

### Materials

Ammonium tungsten oxide ($(NH_4)_2WO_4$) was purchased from Alfa Aesar Co. Ltd. and zinc acetate dihydrate ($(CH_3COO)_2Zn{\cdot}2H_2O$) was purchased from Merck Specialities Private Ltd. and antimony trioxide ($Sb_2O_3$) was purchased from Nice Chemicals Pvt. Ltd. Ethylene glycol ($C_2H_6O_2$) is used as solvent. All the chemicals were used as received, with no further purification.

### Synthesis of Antimony-Zinc Tungstate (ZWS)

The 0.3012 g of $(NH_4)_2WO_4$, 0.512 g $(CH_3COO)_2Zn{\cdot}2H_2O$ and 6.946 mg of $Sb_2O_3$ were dissolved separately in a solution of distilled water and ethylene glycol (1:1 volume ratio). The solutions of antimony trioxide and zinc acetate dihydrate were added to the ammonium tungsten oxide solution and stirred well for 15 min. This reaction mixture was then transferred to a Teflon jar for hydrothermal treatment at 180°C. After 24 h the system was switched off and cooled down to room temperature. The precipitate was separated and washed with distilled water and acetone several times.

To prepare Sb-doped Zinc Tungstate-GO composite, the procedure for the synthesis of Antimony-Zinc tungstate was repeated followed by the addition of 5 mg GO (Modified Hummers method was used to prepare graphene oxide as explained in our previous reports[41]), and the sample is named as ZWS-5.

### Preparation of Working Electrode

The working electrodes for the supercapacitor were prepared using a slurry obtained by mixing the polyvinylidene fluoride (PVDF), carbon black and active material in the ratio of 70:15:15 with some quantity of *N*-methyl-2-pyrrolidone (NMP) being coated on the cleaned titanium foil ($1 \times 1\ cm^2$) and dried overnight in an oven at 60°C. Electrochemical tests were performed using a three electrode system of Biologic SP-150 electrochemical workstation using coated titanium foil as a working electrode, Ag/AgCl as the reference electrode and platinum wire as the counter electrode. The electrochemical properties of the prepared samples were evaluated using cyclic voltammetry (CV), galvanostatic charge–discharge (GCD) and electrochemical impedance spectroscopy (EIS) in 2 M KOH aqueous electrolyte.

### Characterizations

The crystal structure of the prepared sample was characterized by x-ray diffractometer (XRD, Rigaku miniflex 600 XRD instrument) at the scan rate of 2°/min in the $2\theta$ range 10–80°. The micro structure study of the prepared sample was done by a Scanning Electron Microscope (SEM). The optical properties were studied using photoluminescence and UV–visible spectroscopy.

## RESULT AND DISCUSSION

### Powder X-ray Diffraction

Figure 1 indicates the XRD patterns of the r-GO, ZWS and ZWS-5 nanocomposites, which were analysed and indexed by means of Panalytical Xpert high score plus software. The XRD pattern of ZWS shows a Wolframite structure of Sanmartinite and cubic structure, which indicates that Sb formed a separate cubic phase in the sample. $ZnWO_4$ and Sb phases were indexed using JCPDS Card no. 01-073-0554 and 00-017-0125, respectively. In r-GO we can observe a broad peak at around 20° to 25° which confirms the formation of the reduced graphene oxide. In composite we can observe peaks of $ZnWO_4$ and Sb along with reduced graphene oxide.

### Morphology of the Samples

The morphology of the prepared samples was studied using FESEM. We can observe a sheet-like structure for a graphene oxide, which is shown in Fig. 2a. From Fig. 2b we can observe a nanorod-like structure of pure ZWS. ZWS nanorods are formed and grown on r-GO sheets and r-GO sheets are wrapped around the ZWS nanorods, which is clear from Fig. 2c.

The specific surface area of ZWS-5 has increased because of the incorporation of r-GO with ZWS nanorods. It has a specific surface area of 48.607 ($m^2\ g^{-1}$) which is greater than that of pure ZWS and

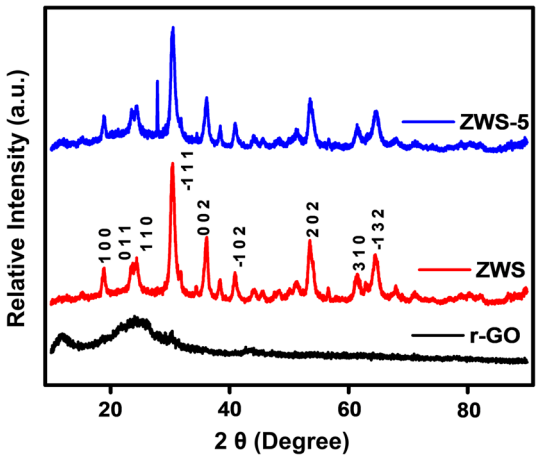


Fig. 1. Powder x-ray diffraction patterns of the r-GO, ZWS and ZWS-5.

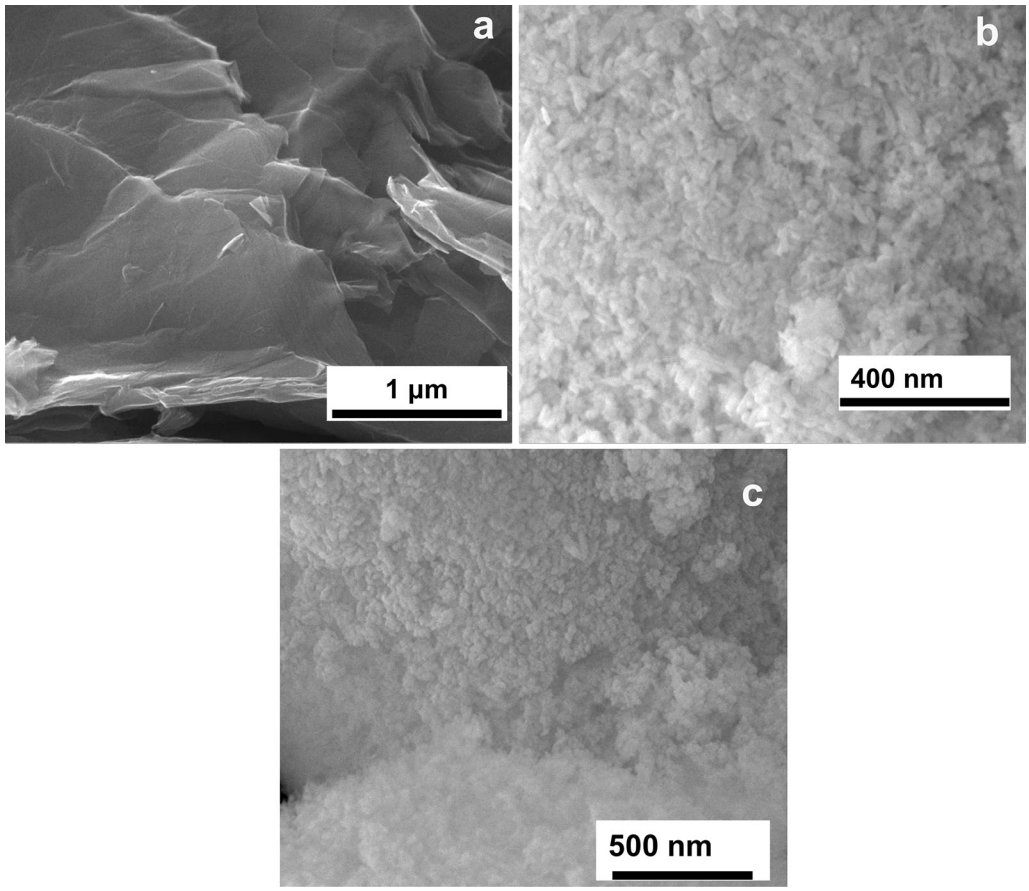


Fig. 2. FESEM images of the prepared (a) r-GO, (b) ZWS and (c) ZWS-5.

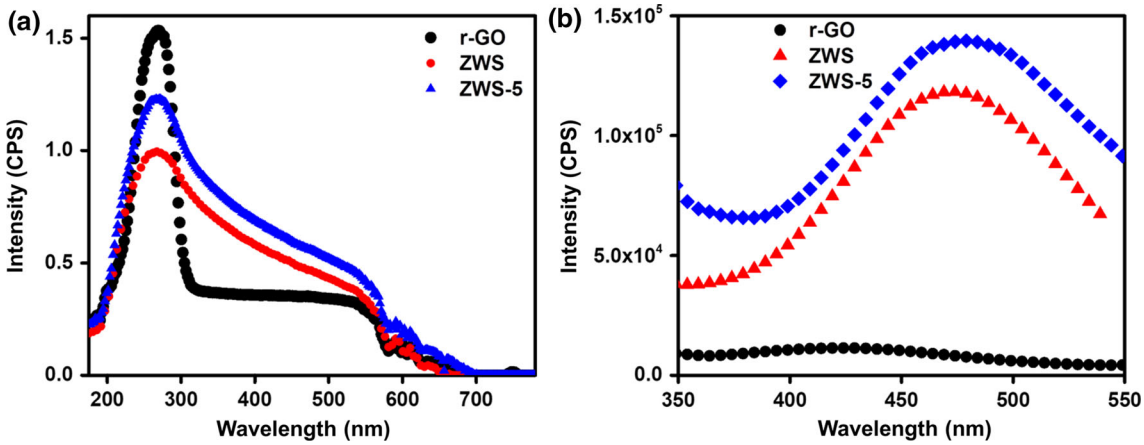


Fig. 3. (a) Absorption spectra and (b) Emission spectra of the prepared r-GO, ZWS and ZWS-5 nanocomposite.

r-GO (16.408 and 46.432 $m^2\ g^{-1}$) respectively. (See supplementary Figure S1 and Table SI).

## Absorption and Emission Spectra

The absorption spectra of the prepared r-GO, ZWS and ZWS-5 composites are given in Fig. 3a. Prepared r-GO, ZWS and ZWS-5 nanocomposites have an absorbance in the UV region with an absorption edge of about 267 nm.

The energy band gap of the prepared samples was estimated using the plot of $(\alpha h\nu)^2$ versus $(h\nu)$ by indirect band gap method as shown in Fig. 4. From the below equation, the conduction band ($E_c$) and valence band ($E_v$) of $ZnWO_4$ can be calculated.[42,43]

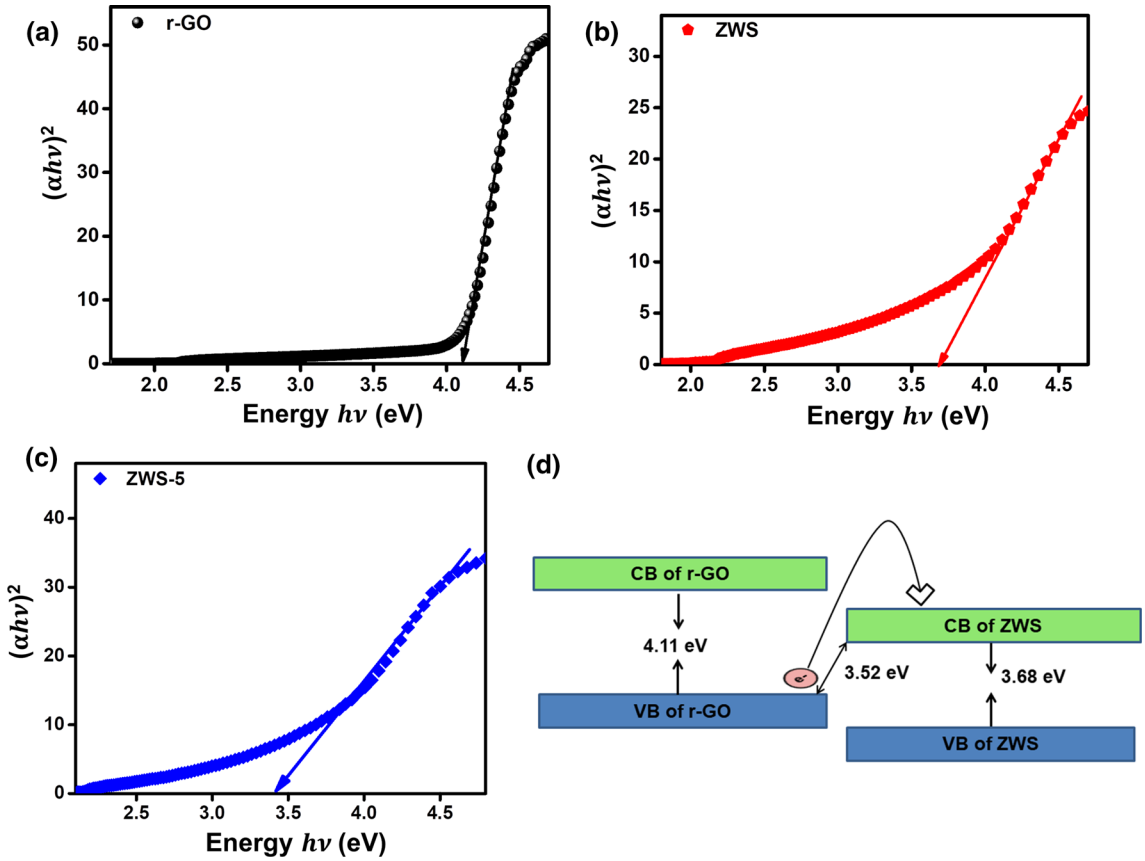


Fig. 4. Tauc plot analysis of the (a) r-GO, (b) ZWS, (c) ZWS-5 nanocomposite samples and (d) schematic representation of $E_g$ values.

**Table I. Obtained Energy band gap from the $(\alpha h\nu)^2$ Vs $(h\nu)$ plot**

| Compound | $E_g$ (eV) obtained | $E_g$ (eV) literature | References |
|---|---|---|---|
| r-GO | 4.11 | 4.9–0.02 | Refs. 44–46 |
| ZWS | 3.68 | 3.25–4.4 | Refs. 47, 48 |
| ZWS-5 | 3.52 | 3–3.7 | Refs. 49–51 |

$$E_c = E_v - E_g \quad (1)$$

$$E_v = X - E_c + 0.5E_g, \quad (2)$$

where $X$ is the electronegativity $X = (X(\mathrm{Zn})X(\mathrm{W})X(\mathrm{O})^4)^{1/6}$. While Zn, O and W atoms have electronegativity values of 4.45 eV, 7.54 eV and 4.40 eV, respectively. Then the calculated value of $X$ is 6.31 eV. The value of $E_c$ is 4.5 EV, which is the energy of free electrons in a hydrogen atom. The conduction band ($E_c$) and valence band ($E_v$) of the $ZnWO_4$ are 3.65 eV and − 0.03 eV, respectively. The obtained band gap values of the prepared samples from the $(\alpha h\nu)^2$ versus $(h\nu)$ plot and their comparison with the reported values are given in the Table I.

The ZWS-5 nanocomposite shows a comparatively higher absorption than that of ZWS. This may be due to the synergic interactions of r-GO and ZWS in the composite. From Table I, we can observe that, there is a reduction in the band gap. This may possibly be due to the surface charge delocalization brought about by the interaction of r-GO and ZWS in the composite. Such interpretations for a semiconductor composite was stated in the literature.[50,51] Schematic diagram of delocalization of charges is shown in Fig. 4d.

The emission spectra of the prepared r-GO, ZWS and ZWS-5 nanocomposite are shown in Fig. 3b. The photoluminescence (PL) emission was recorded for the prepared r-GO, ZWS and ZWS-5 with the excitation wavelength of 260 nm. The PL emission signal arises from the recombination of excited electrons and holes. The PL spectrum of ZWS has a broad emission with peak value of 475 nm (2.61 eV) but there is no emission peak for r-GO. Whereas in the ZWS-5 nanocomposite, there is a shift in emission peak at 487 nm (2.54 eV). The

ZWS-5 composite has a broader emission peak than ZWS due to the transfer of photoinduced electrons from the trapped states of ZWS to the r-GO nanosheets. These observations suggest that the combination of ZWS and r-GO can enhance the recombination of excited electrons and holes.

## Electrochemical Supercapacitor

Figure 5a presents the CV curves of the ZWS and ZWS-5 nanocomposite samples at a scan rate of 100 mV/s using a three electrode system in 2 M KOH electrolyte at a potential range of − 0.6–0.2 V. The absolute area of the CV curve is higher for prepared ZWS-5 nanocomposite than pristine ZWS due to the incorporation of r-GO. The specific capacitance ($C_s$) of the prepared samples at different scan rates was calculated using Equation [52]

$$C_s = \frac{\int I(V)\mathrm{d}v}{mv\Delta V}, \tag{3}$$

where $C_s$ (F/g) is the specific capacitance, $m$ (mg) is the mass of the active material, $v$ (mV/s) is the scan rate and $\Delta V$ (volts) is the potential window. The specific capacitances of the ZWS and ZWS-5 are obtained as 64 F/g and 102 F/g at a scan rate of 1 mV/s. The increase of the specific capacitance is due to r-GO. The incorporation of r-GO enhances the surface area, conductivity and improvement in the properties of the composites results in the increment in the specific capacitance of the composite. The composite is one of the best materials for the supercapacitor electrode compared to other metal tungstates. The comparison with other metal tungstates was tabulated in Table II.

Figure 5b and c represent the CV curves of ZWS and ZWS-5 at different scanning rates of 1 mV/s, 5 mV/s, 25 mV/s, 75 mV/s and 100 mV/s, respectively. The figure clearly depicts the increase in the area under the curve with respect to scan rate. For the lower scan rate, capacitance increases due to absorption and desorption of the ions at available sites. In the lower scan rate the ions diffuse and get absorbed at accessible sites which increase the specific capacitance of the material.[58]

Figure 5d shows the charge–discharge curve of the ZWS and ZWS-5 at 1 A/g. The electrodes represent the triangular symmetrical curves, which demonstrate the supercapacitor behavior. As seen in Fig. 5d, ZWS-5 structure shows the longest

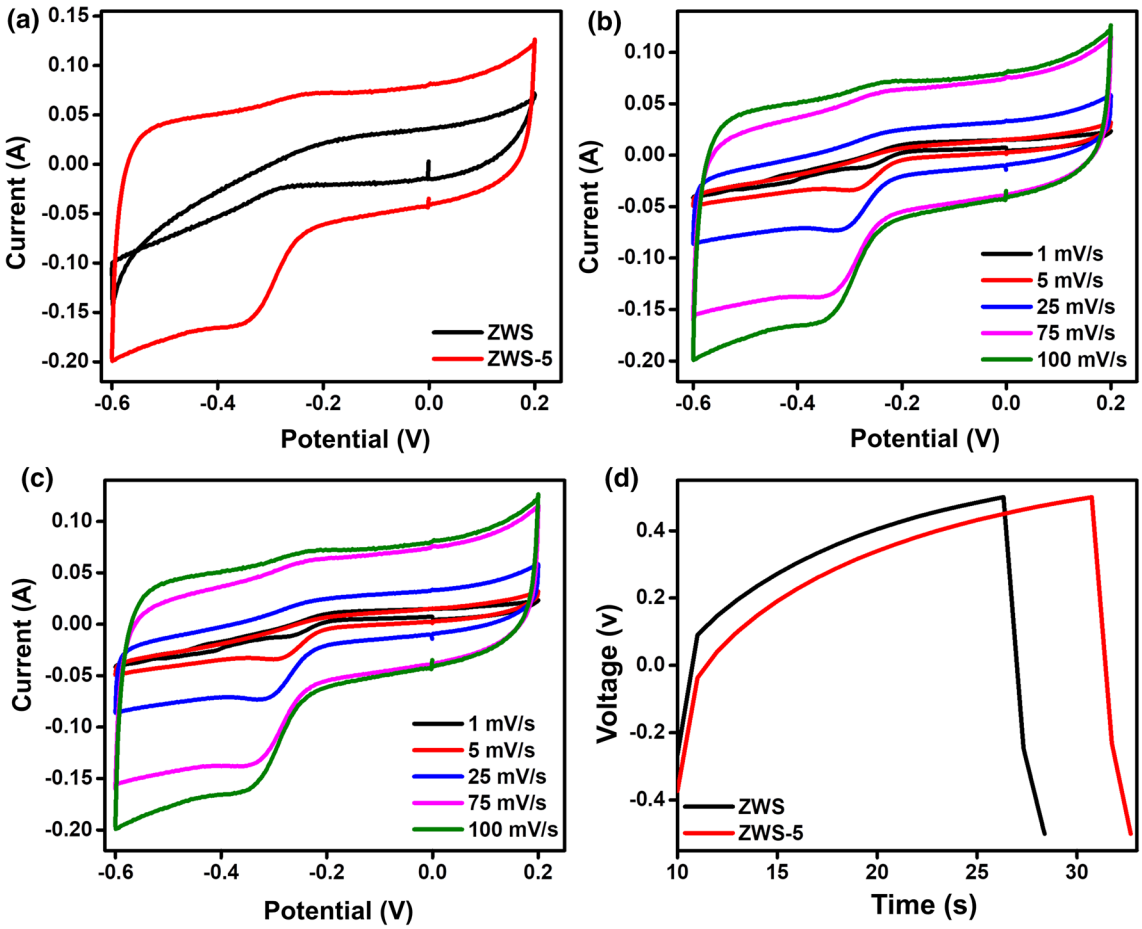


Fig. 5. (a) CV of the ZWS and ZWS-5 nanocomposite at a scan rate of 100 mV/s. (b) and (c) CV of the ZWS and ZWS-5 at different scan rates. (d) Charge–discharge curve of the ZWS and ZWS-5 nanocomposite at 1 A/g.

charge–discharge period, compared to ZWS, providing the highest capacitance.

Figure 6 shows the band gap and the specific capacitance plot. The specific capacitance and band gaps of the ZWS and ZWS-5 nanocomposite are 64 F/g, 102 F/g, 3.68 eV and 3.52 eV, respectively. From Fig. 6 it is clear that, the specific capacitance is negatively correlated to the energy band gap of the material. The decrease in the band gap increases the electrochemical performance of the ZWS in accordance with the incorporation of reduced graphene oxide. The graphene oxide content can create bonding and anti-bonding bands which are related to hybridization of empty and occupied defect states. This transports more л electrons and improves the conductivity. During the charging–discharging process, the good conductivity can rush the transport and relocate electrolyte ions or electrons in the ZWS.[38,59,60] The lower band gap and incorporation of r-GO enhances the capacitance of the ZWS-5 nanocomposite.

To find the kinetics of the electrode material, EIS were performed in the frequency range of 0.1 Hz to 1 MHz in a 2 M KOH electrolyte besides Ag/AgCl as the reference electrode and Pt wire as counter electrode. Figure 7a represents the Nyquist plot of the prepared ZWS and ZWS-5 electrodes. It is notable that, at high frequency, the supercapacitor exhibits resistive behavior while at a lower frequency it exhibits capacitive behavior.[61,62] Generally, Nyquist curves provide information about capacitors and the resistor behavior of the material. A vertical straight line at a lower frequency region explains the capacitor behavior of the electrode and the kinetic arc at a higher frequency region explains the resistive behavior. From Fig. 7a, the Nyquist plot of the electrodes exposes the semicircles due to the charge transfer resistance at the electrode and electrolyte interface. For ZWS-5 a nanocomposite semicircle was decreased due to incorporation of r-GO, which specifies the decrease in the charge transfer resistance. Figure 7c shows the simple Randles circuit fitted to the Nyquist plot. Values of the solution resistance ($R_s$), charge transfer resistance ($R_{ct}$) and double layer capacitance ($C_{dl}$) are tabulated in Table III for the electrodes.

Figure 7b illustrates the capacitance retention of the prepared ZWS and ZWS-5 nanocomposite. For ZWS, capacity is gradually reduced, and it has 52% retention at the 1000th cycle. While for ZWS-5 it reduces to 67% at the 100th cycle, and there is no

**Table II. The comparison of the specific capacitance with other metal tungstate Nanomaterials**

| | $C_s$ (F/g) | Scan rate ( mV/s) | Electrolyte | References |
|---|---|---|---|---|
| $ZnWO_4$ nanoparticles | 72 | 5 | 3 M KOH | Ref. 53 |
| $MnWO_4$ nanorods | 27 | 5 | 1 M $H_2SO_4$ | Ref. 54 |
| $MnWO_4$ | 68 | 5 | 6 M KOH | Ref. 55 |
| $MnWO_4$ | 18 | 5 | 1 M $H_2SO_4$ | Ref. 56 |
| $FeWO_4$ | 8 | 10 | 3 M NaCl | Ref. 57 |
| ZWS | 64 | 1 | 2 M KOH | Present work |
| ZWS-5 | 102 | 1 | 2 M KOH | Present work |

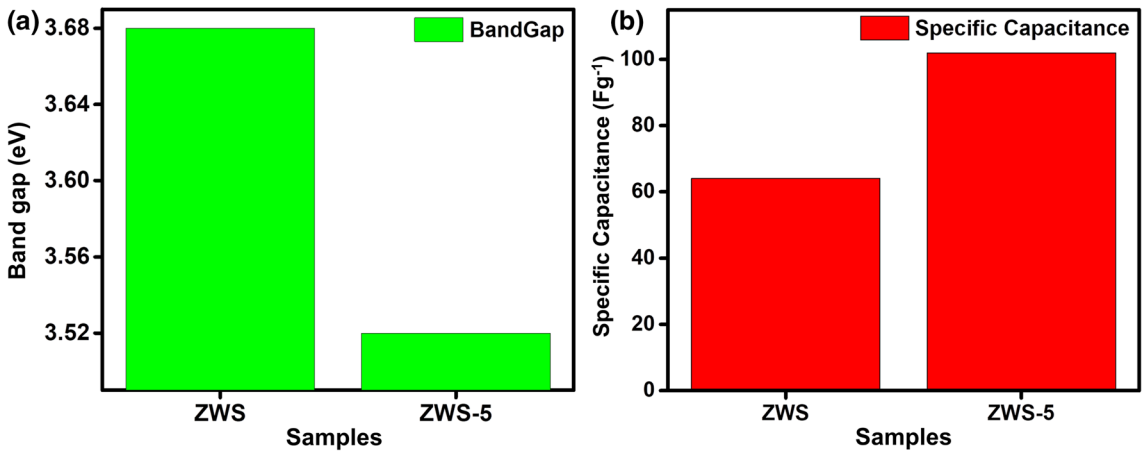


Fig. 6. The band gap and specific capacitance of the ZWS and ZWS-5 nanocopmposite electrodes.

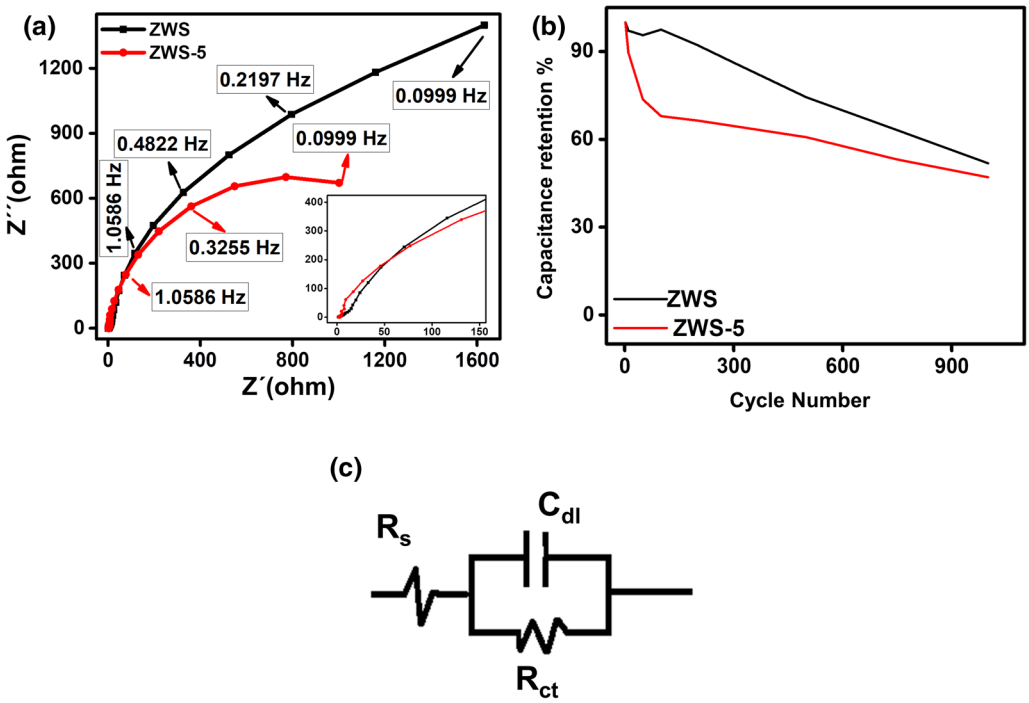


Fig. 7. (a) Nyquist plot of the ZWS and ZWS-5 electrodes, (b) Cyclic stability of the sample and (c) equivalent circuit for the Nyquist plot.

**Table III. Capacitance and solution resistance calculated from the Nyquist plot**

| Samples | Solution resistance ($R_s$) Ω | Charge transfer resistance ($R_{ct}$) Ω | Double layer capacitance ($C_{dl}$) μF |
|---|---|---|---|
| ZWS | 1.435 | 5467 | 153.5 |
| ZWS-5 | 1.036 | 2308 | 431 |

significant reduction till 500 cycles, then it has reduced to 47% at the 1000th cycle.

## CONCLUSION

Solvothermally prepared Sb/$ZnWO_4$/r-GO nanocomposite has Sb/$ZnWO_4$ nanorods of monoclinic wolframite structure. The specific capacitance of Sb/$ZnWO_4$ nanorods and Sb/$ZnWO_4$/r-GO nanocomposite are 64 F/g and 102 F/g, respectively. The incorporation of r-GO nanosheets with Sb/$ZnWO_4$ nanorods enhances the specific surface area of Sb/$ZnWO_4$ nanorods, thereby it increases the electrochemical activity. Also, the band gap and charge transfer resistance ($R_{ct}$) of Sb/$ZnWO_4$ have been reduced on addition of r-GO nanosheets, which contribute to the enhancement of electrochemical activity of the composite.

## ACKNOWLEDGMENTS

Authors would like to thank DST-FIST India for providing the XRD facility of the Department of Physics NITK Surathkal.

## ELECTRONIC SUPPLEMENTARY MATERIAL

The online version of this article (https://doi.org/10.1007/s11664-019-07185-8) contains supplementary material, which is available to authorized users.

## REFERENCES

1. N. Shi, S. Xiong, W. Fangfang, J. Bai, Y. Chu, H. Mao, J. Feng, and B. Xi, *Eur. J. Inorg. Chem.* 2017, 734 (2017).
2. Y. Yang, J. Zhu, W. Shi, J. Zhou, D. Gong, G. Shaozhen, L. Wang, X. Zhi, and L. Binan, *Mater. Lett.* 177, 34 (2016).
3. J. Libich, J. Máca, J. Vondrák, O. Čech, and M. Sedlaříková, *J. Energy Storage* 17, 224 (2018).
4. A. González, E. Goikolea, J.A. Barrena, and R. Mysyk, *Renew. Sustain. Energy Rev.* 58, 1189 (2016).
5. T. Purkait, G. Singh, D. Kumar, M. Singh, and R.S. Dey, *Sci. Rep.* 8, 640 (2018).
6. Q. Ke and J. Wang, *J. Materiomics* 2, 37 (2016).
7. R. Boddula, R. Bolagam, and P. Srinivasan, *Ionics* 24, 1467 (2018).
8. W. Yu and C. Cao, *Sci. China Mater.* 61, 1517 (2018).
9. T. Hao, W. Wang, and Yu Dan, *J. Electron. Mater.* 47, 4108 (2018).

10. Q. Meng, K. Cai, Y. Chen, and L. Chen, *Nano Energy* 36, 268 (2017).
11. G.A. Snook, P. Kao, and A.S. Best, *J. Power Sour.* 196, 1–12 (2011).
12. I. Shown, A. Ganguly, L.-C. Chen, and K.-H. Chen, *Energy Sci. Eng.* 3, 2 (2015).
13. K.D. Fong, T. Wang, and S.K. Smoukov, *Sustain. Energy Fuels* 1, 1857 (2017).
14. C.C. Chang and T. Imae, *ACS Sustainable Chemistry & Engineering* 6, 5162 (2018).
15. Y.N. Sudhakar and M. Selvakumar, *Ionics* 22, 1729 (2016).
16. T.P. Tran and Q.H. Do, *J. Electron. Mater.* 46, 6056 (2017).
17. S. Ghosh, S.M. Jeong, and S.R. Polaki, *Korean J. Chem. Eng.* 35, 1389 (2018).
18. Y. Liu, L. Liu, L. Kong, L. Kang, and F. Ran, *Electrochim. Acta* 211, 469 (2016).
19. J. Theerthagiri, G. Durai, K. Karuppasamy, P. Arunachalam, V. Elakkiya, P. Kuppusami, T. Maiyalagan, and H.S. Kim, *J. Ind. Eng. Chem.* 67, 12 (2018).
20. M.-S. Balogun, W. Qiu, W. Wang, P. Fang, L. Xihong, and Y. Tong, *J. Mater. Chem. A* 3, 1364 (2015).
21. Y. Zhong, X. Xia, F. Shi, J. Zhan, J. Tu, and H.J. Fan, *Adv. Sci.* 3, 1500286 (2016).
22. P. Liu, Y. Deng, Q. Zhang, H. Zhonghua, X. Zijie, Y. Liu, M. Yao, and Z. Ai, *Ionics* 21, 2797 (2015).
23. H. Zhang, J. Liu, Z. Tian, Y. Ye, Y. Cai, C. Liang, and K. Terabe, *Carbon* 100, 590 (2016).
24. Y. Zhao, W. Wang, D.-B. Xiong, G. Shao, W. Xia, Yu Shengxue, and F. Gao, *Int. J. Hydrogen Energy* 37, 19395 (2012).
25. B. Krüner, C. Odenwald, A. Tolosa, A. Schreiber, M. Aslan, G. Kickelbick, and V. Presser, *Sustain. Energy Fuels* 1, 1588 (2017).
26. M.R. Lukatskaya, S. Kota, Z. Lin, M.-Q. Zhao, N. Shpigel, M.D. Levi, J. Halim, P.-L. Taberna, M.W. Barsoum, P. Simon, and Y. Gogotsi, *Nat. Energy* 2, 17105 (2017).
27. A. Sanger, A. Kumar, A. Kumar, P.K. Jain, Y.K. Mishra, and R. Chandra, *Ind. Eng. Chem. Res.* 55, 9452–9458 (2016).
28. B. Guan, H. Lingling, G. Zhang, D. Guo, F. Tao, J. Li, H. Duan, C. Li, and Q. Li, *RSC Adv.* 4, 4212 (2014).
29. V. Sharma, I. Singh, and A. Chandra, *Sci. Rep.* 8, 1307 (2018).
30. L. Wang, G. Duan, J. Zhu, S.-M. Chen, X.-h. Liu, and S. Palanisamy, *J. Colloid Interface Sci.* 483, 73 (2016).
31. M. Aliofkhazraei, A.S.H. Makhlouf, eds., *Handbook of nanoelectrochemistry: Electrochemical synthesis methods, properties and characterization techniques* (Springer, 2016).
32. K. Zhang, L. Lin, S. Hussain, and S. Han, *J. Mater. Sci. Mater. Electron.* 29, 12871 (2018).
33. S. Sun, G. Jiang, Y. Liu, Yu Bo, and U. Evariste, *J. Electron. Mater.* 47, 5993 (2018).
34. X. Zhou, M. Wang, J. Lian, and Y. Lian, *Sci. China Technol. Sci.* 57, 278 (2014).
35. C. Chen, W. Fan, T. Ma, and F. Xuwang, *Ionics* 20, 1489 (2014).
36. J.V. Moreira, P.W. May, E.J. Corat, A.C. Peterlevitz, R.A. Pinheiro, and H. Zanin, *J. Electron. Mater.* 46, 929 (2017).
37. J.V.S. Moreira, E.J. Corat, P.W. May, L.D.R. Cardoso, P.A. Lelis, and H. Zanin, *J. Electron. Mater.* 45, 5781 (2016).
38. S. Wang, F. Ma, H. Jiang, Y. Shao, W. Yongzhong, and X. Hao, *ACS Appl. Mater. Interfaces.* 10, 19588 (2018).
39. S. Saha, M. Jana, P. Khanra, P. Samanta, H. Koo, N.C. Murmu, and T. Kuila, *RSC Adv.* 6, 1380 (2016).
40. S. Saha, M. Jana, P. Samanta, N.C. Murmu, N.H. Kim, T. Kuila, and J.H. Lee, *Mater. Chem. Phys.* 190, 153 (2017).
41. M. Sreejesh, N.M. Huang, and H.S. Nagaraja, *Electrochim. Acta* 160, 94 (2015).
42. Y. Li, F. Zhou, Z. Zhu, and W. Fan, *Appl. Surf. Sci.* 467–468, 819 (2019).
43. J. Jin, Yu Jiaguo, D. Guo, C. Cui, and W. Ho, *Small* 11, 5262 (2015).
44. M.A. Velasco-Soto, S.A. Pérez-García, J. Alvarez-Quintana, Y. Cao, L. Nyborg, and L. Licea-Jiménez, *Carbon* 93, 967 (2015).
45. K.Y. Lian, Y.F. Ji, X.F. Li, M.X. Jin, D.J. Ding, and Y. Luo, *J. Phys. Chem. C* 117, 6049 (2013).
46. M. Singh, G. Kumar, N. Prakash, S.P. Khanna, P. Pal, and S.P. Singh, *Semicond. Sci. Technol.* 33, 045012 (2018).
47. R. Lacomba-Perales, J. Ruiz-Fuertes, D. Errandonea, D. Martínez-García, and A. Segura, *EPL (Europhys. Lett.)* 83, 37002 (2008).
48. P. Siriwong, T. Thongtem, A. Phuruangrat, and S. Thongtem, *CrystEngComm* 13, 1564 (2011).
49. J. Lin, J. Lin, and Y. Zhu, *Inorg. Chem.* 46, 8372 (2007).
50. M.M.J. Sadiq, U.S. Shenoy, and D.K. Bhat, *RSC Adv.* 6, 61821 (2016).
51. M.J.S. Mohamed and D.K. Bhat, *AIMS Mater. Sci.* 4, 158 (2017).
52. K. Bindu, K. Sridharan, K.M. Ajith, H.N. Lim, and H.S. Nagaraja, *Electrochim. Acta* 217, 139 (2016).
53. S.R. Ede, A. Ramadoss, U. Nithiyanantham, S. Anantharaj, and S. Kundu, *Inorg. Chem.* 54, 3851 (2015).
54. S. Saranya, S.T. Senthilkumar, K.V. Sankar, and R.K. Selvan, *J. Electroceram.* 28, 220 (2012).
55. J. Tang, J. Shen, N. Li, and M. Ye, *J. Alloy. Compd.* 666, 15 (2016).
56. S. Saranya, R.K. Selvan, and N. Priyadharsini, *Appl. Surf. Sci.* 258, 4881 (2012).
57. N. Goubard-Bretesché, O. Crosnier, C. Payen, F. Favier, and T. Brousse, *Electrochem. Commun.* 57, 61 (2015).
58. M. Sreejesh, S. Dhanush, F. Rossignol, and H.S. Nagaraja, *Ceram. Int.* 43, 4895 (2017).
59. Y. Li Sun, C. Tian, Y. Yang, L. Wang, J. Yin, J. Ma, R. Wang, and F. Honggang, *Chemsuschem* 7, 1637 (2014).
60. D. Deng, N. Chen, X. Xiao, D. Shangfeng, and Y. Wang, *Ionics* 23, 121 (2017).
61. K.S. Bhat, S. Shenoy, H.S. Nagaraja, and K. Sridharan, *Electrochim. Acta* 248, 188 (2017).
62. K. Brijesh, K. Bindu, D. Shanbhag and H. S. Nagaraja, *Int. J. Hydrogen Energy* 44(2), 757–767 (2018). https://doi.org/10.1016/j.ijhydene.2018.11.022.


**Publisher's Note** Springer Nature remains neutral with regard to jurisdictional claims in published maps and institutional affiliations.